

© 2016 Rui Su

SUPERSONIC COOLING OF SHORT-LIVED MOLECULAR STATES IN
A PULSED MICROCAVITY PLASMA JET

BY

RUI SU

THESIS

Submitted in partial fulfillment of the requirements
for the degree of Master of Science in Electrical and Computer Engineering
in the Graduate College of the
University of Illinois at Urbana-Champaign, 2016

Urbana, Illinois

Adviser:

Professor J. Gary Eden

ABSTRACT

Electronic states of helium dimers having potential energy > 24 eV and radiative lifetimes as short as 19 ns have been generated in a micro-plasma jet at super-atmospheric pressure and rotationally cooled by supersonic expansion. Spatial-temporal spectrograms of $d^3\Sigma_u^+ \rightarrow b^3\Pi_g$ (v', v'') = (0, 0) emission are obtained, which contain the information about the dynamic cooling process during the molecular beam expansion. Analysis shows the spatial-temporal evolution of the rotational temperature to be a damped sinusoid that reaches a minimum value of 100 K, which is attributed to the reflection of electrons from a virtual cathode located downstream of the jet nozzle. Data fitting to the damped sinusoid function yields a spatially-averaged electron density of 10^8 cm^{-3} . The experimental setup has the potential to be used in exploration of the spectroscopy and plasma dynamics in various gas molecules.

ACKNOWLEDGMENTS

The author would like to give thanks to Professor J. Gary Eden for his teaching, advising, and his graceful trust, support and patience without which this thesis is not possible. Special thanks to Thomas Houlahan, Jr., the pioneer of this project, who taught me so much not only in knowledge, but also in the habits and attitude of being a scientific researcher. Many thanks to Jose Rivera, Thomas Galvin, Andrey Mironov, Kyle Raymond, and Wenting Chen for their numerous acts of help and support in the lab. I am privileged to call them friends and colleagues. Outside of academics, I am also very grateful to Betoel and Margaret Escobar, Daniel Escobar, Benjamin Escobar, Bob and Ruth Chesnut, Jon Bair and Joel Mackinney. I believe they contributed to this thesis in an invisible way. Last but not least, thanks to my mom and dad. I am blessed by God for being your son.

TABLE OF CONTENTS

CHAPTER 1	INTRODUCTION	1
CHAPTER 2	THEORETICAL BACKGROUND	3
2.1	Supersonic expansion	3
2.2	Energy structure of He_2	5
CHAPTER 3	EXPERIMENT	8
3.1	Microcavity plasma jet	8
3.2	Experimental arrangement	8
3.3	Two main emission stages	9
3.4	Emission spectrogram of helium dimers	11
CHAPTER 4	ANALYSIS	13
4.1	Rotational temperature analysis of He_2 $d^3\Sigma_u^+ \rightarrow b^3\Pi_g(v', v'') =$ $(0, 0)$ emission	13
4.2	Damped harmonic oscillation in rotational temperature cooling	16
CHAPTER 5	CONCLUSIONS	20
REFERENCES	21

CHAPTER 1

INTRODUCTION

The study of atomic and molecular beams played an important role in modern physics for more than 100 years. To name a few contributions, its development has been associated with the the verification of the Maxwell-Boltzmann velocity distribution of gaseous atoms (O. Stern, 1911), nuclear magnetic resonance (I. Rabi, 1938), fine structure in electronically excited H atom (W. Lamb and R. Retherford, 1947), the precursor of the development of quantum electrodynamics theory [1]. The technique of using supersonic beams joined the arena in 1951 [2] by offering molecular beams with well-defined density and kinetic energy, and its unique cooling effect. With the help of lasers, supersonic beams further advanced the study of molecular spectroscopy. We employ the cooling ability of supersonic molecular beams in this research. The cooling drastically simplifies the emission or absorption spectrum, by compressing the population into the lowest vibrational-rotational levels.

On the other hand, microcavity plasma technology was developed more than ten years before this thesis was written. It has been proved as an efficient method to generate transient molecules like rare gas dimers that are hard to obtain in traditional plasma devices or by optical methods [3]. According to Paschen's law [4, 5], reducing the distance between the discharge electrodes increases the operating gas pressure under certain breakdown voltage, enhancing the collisions between gas molecules that contribute to certain physical processes, such as three-body collisions.

Aiming to discover new phenomenon in molecular spectroscopy and plasma physics, this research combines the advantages of the two techniques discussed above. We utilize a microcavity plasma device to generate electronic molecular states that have excitation energies at least 24 eV and very short radiative lifetimes and employ supersonic cooling to simplify, "decongest" the emission spectrum of these highly excited molecules.

In our experiment, helium dimers with highly excited electronic states

are generated, rotationally cooled while expanding in the vacuum, and the processes of which are recorded by capturing spectrograms that change with time and space.

We have obtained the spectrograms of $d^3\Sigma_u^+ \rightarrow b^3\Pi_g(v', v'') = (0, 0)$, $f^3\Sigma_u^+ \rightarrow b^3\Pi_g(v', v'') = (0, 0)$ and $e^3\Pi_g \rightarrow a^3\Sigma_u^+(v', v'') = (0, 0)$ emissions in helium dimers. Analysis of the $d^3\Sigma_u^+ \rightarrow b^3\Pi_g(v', v'') = (0, 0)$ emission shows the spatial-temporal evolution of the rotational temperature to be a damped sinusoid that reaches a minimum value of 100 K. This reproducible behavior is attributed to a virtual cathode located downstream of the expansion. A fitting of the model yields a spatially-averaged electron density of 10^8 cm^{-3} .

CHAPTER 2

THEORETICAL BACKGROUND

2.1 Supersonic expansion

Over the decades, supersonic molecular beams have remained a useful technique to facilitate the study of molecular spectroscopy and found numerous applications in a broader field of research in atomic and molecular physics [1]. Supersonic expansion has additional benefits including the ability to prepare the molecules under inspection with very low internal temperature so that the absorption or emission spectrum becomes less congested and more interpretable. Detailed discussion of this “cooling effect” can be found in other sources, e.g. [1,2,6] but will be briefly discussed here.

As shown in Figure 2.1, an opening orifice on the gas reservoir connects the high pressure gas to the vacuum environment. If the dimension of the orifice is much larger than the mean free path of the gas molecules in the reservoir, but not large enough to spoil the vacuum, the molecules experience a number of collisions during their expansion, which converts internal energy of the molecule into directed kinetic energy. This energy conversion can be quantitatively written in the following equation, assuming an adiabatic

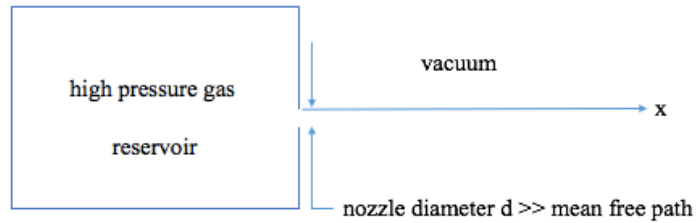


Figure 2.1: Illustration of supersonic expansion. High pressure gas is released into the vacuum via an orifice on the reservoir.

and isentropic process by neglecting gas viscosity and heat transfer with the environment,

$$H(T) + \frac{1}{2}u(x)^2 = H(T_0) \quad (2.1)$$

For the molecular gas, $H(T)$ denotes its enthalpy at location x along the axis of expansion with $x = 0$ at the orifice opening, $\frac{1}{2}u(x)^2$ denotes kinetic energy of molecules in collective motion and T_0 is the initial temperature in the reservoir.

As the molecules expand further away from the orifice, the velocity of the collective movement of the molecules $u(x)$ keeps increasing, while the entropy and internal energy of molecules are decreasing, molecules being cooled. In reality (as we will see Chapter 4), the system is not in thermal equilibrium and has to be described by different temperatures in terms of translational, rotational, vibrational and electronic energies. Since the energy differences between adjacent levels are increasing in the following sequence,

$$\text{translational} < \text{rotational} < \text{vibrational} < \text{electronic}$$

the translational temperature is cooled most efficiently. Less efficient is the cooling of rotational and vibrational temperatures, and at last, almost no cooling in electronic temperature. The concept of temperature cooling can be easier to understand when we evoke that the term “temperature” in a microscopic sense means how randomly the molecules move in certain modes of motion. When the more random translational motion of the molecules is converted into a more directed translational motion, the translational temperature is decreased.

For an ideal gas under thermal equilibrium, the depth of cooling is related to the depth of drop in the pressure, as follows [6],

$$\frac{T_1}{T_0} = \left(\frac{p_1}{p_0}\right)^{(\gamma-1)/\gamma}; \quad \frac{\rho_1}{\rho_0} = \left(\frac{p_1}{p_0}\right)^{(1/\gamma)}; \quad \frac{\rho_1}{\rho_0} = \left(\frac{T_1}{T_0}\right)^{1/(\gamma-1)} \quad (2.2)$$

where P , T and ρ refer to pressure, temperature and gas density, respectively. Subscripts $_0$ and $_1$ represent the initial and final states. In conclusion, a large reduction in temperature requires a large pressure difference.

For ideal gas, the speed of sound a is proportional to the local gas temperature, given by,

$$a(T) = \sqrt{\frac{\gamma RT}{m}} \quad (2.3)$$

A term related to the speed of sound and commonly encountered in gas cooling is the Mach number, M , defined as $M(x) = u(x)/a(x)$. Apparently, the Mach number increases as the temperature reduces because the speed of sound decreases. When $M(x)$ is larger than unity, the expansion becomes supersonic. Mach numbers of 20 or greater are typical in supersonic expansion [6].

2.2 Energy structure of He₂

The energy structure of a diatomic molecule can be understood by Born-Oppenheimer approximation. Because the mass of electrons is much smaller than that of the nuclei, under Born-Oppenheimer approximation the nuclei and the internuclear distance are assumed to be fixed when studying the behavior of electrons. As a result, the energy of a particular quantum state can be approximated as a sum of electronic, vibrational, rotational and translational energies, *i.e.*, $E \simeq E_e + E_v + E_N + E_t$, while the true wave function of the molecule is approximated by a product of electronic, vibrational and rotational wave functions (nuclear part and spins not considered). Under Born-Oppenheimer approximation, quantum mechanic computation yields various potential energy surfaces (PES), the bottoms of which form different electronic states. For diatomic molecules, the bottom of a certain PES can be approximated as parabolic and thus the discrete vibrational energies associated with this electronic state can be modeled using harmonic oscillation,

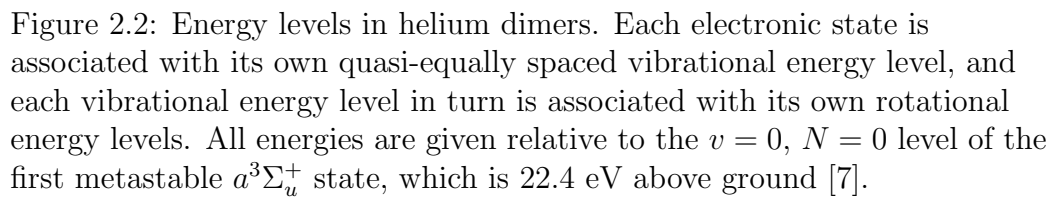
$$E_v(v) = (v + \frac{1}{2})\hbar\omega \quad (2.4)$$

where v denotes vibrational quantum number $v = 0, 1, 2 \dots$, \hbar is the reduced Plank constant and ω is the angular frequency for the vibration determined by the curvature of an electronic potential. For a certain vibrational level, the rotational motion of the nuclei can be modeled on the first order as rigid-rotator, of which the discrete energies levels are given by,

$$E_N(N) = BN(N + 1) = \frac{\hbar^2}{2I}N(N + 1) \quad (2.5)$$

where N is the rotational quantum number $N = 1, 2, 3 \dots$, B is the so-called rotational constant defined as $B = \frac{\hbar^2}{2I}N(N + 1)$ where I is the molecule's moment of inertia.

Figure 2.2 shows some energy levels in He_2 [7]. Each electronic state is designated by a combination of united atom molecular orbitals (UAMOs) and term symbols in the LS coupling scheme. For a detailed discussion on molecular orbital theories, angular momentum coupling scheme and term symbols, refer to books on physical chemistry such as [8] or Herzberg's treatment on the energy structure of diatomic molecules [9]. Note that in Figure 2.2, all energies are given relative to the $v = 0$, $N = 0$ level of the first metastable $a^3\Sigma_u^+$ state, which is 22.4 eV above ground. As a result, for the three electronic states we survey in this research, namely $d^3\Sigma_u^+$, $e^3\Pi_g$, and $f^3\Sigma_u^+$ states, their energy levels are more than 24 eV above ground. Experimentally, these electronic states with relatively high excitation energy are generated in microcavity plasma devices.



CHAPTER 3

EXPERIMENT

3.1 Microcavity plasma jet

A custom-made microcavity plasma device is used in the discharge to excite gas molecules. A schematic diagram of the device's structure is shown in Figure 3.1. The fabrication process is similar to those as described in [10,11]. Two strips of anodized aluminum are bonded together to form two electrodes for the dielectric barrier discharge. The initial thickness of aluminum foil is $250\text{ }\mu\text{m}$ and after the anodization process only $30\text{ }\mu\text{m}$ of the aluminum core is left in each strip. In the last step, the bonded strips are etched all the way through using a sandblaster, yielding a parabolic cross section with a $200\text{ }\mu\text{m}$ diameter opening on the vacuum side. When operating, a pulsed valve is attached to the back of the device to control the gas flow.

3.2 Experimental arrangement

The experimental arrangement is illustrated in Figure 3.2. The device and its attached valve are placed in a vacuum chamber that is pumped to 10^{-7} Torr when the experiment is off. When the device is being discharged at 4 atm backing pressure and 10 Hz frequency (thus the valve will open 10 times in one second), the background pressure within the chamber raises up to approximately 5×10^{-6} Torr, sustaining a big pressure difference to enable supersonic cooling. The driving circuits for the discharge are customly made which incorporate a Blumlein pulse generator and thyatron switch, enabling a 2 kV discharge voltage of 20~30 ns rise time and duration less than 200 ns across the electrodes. In order to obtain a spectrum at each temporal moment downstream of the expansion, lenses and steering mirrors are used to image

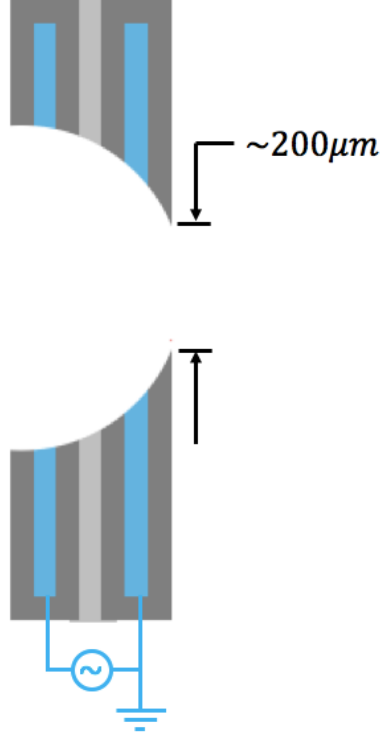


Figure 3.1: Schematic diagram of the microplasma device (dimensions not to scale). The opening on the vacuum side is $\sim 200 \mu m$ in diameter. Following the chemical anodization process, two electrodes are embedded within the oxidized aluminum. They are bonded and etched through using a sandblaster, resulting in a parabolic cross section with a $200 \mu m$ diameter opening on the vacuum side.

the axis of expansion onto the slit of a Czerny-Turner spectrometer with 0.75 m focus length. It is worthy to note that the image of the axis should be in parallel with the slit, so that on the focal plane of the spectrometer an intensified CCD (ICCD) will capture a spectrogram of all locations along the axis of the molecules' expansion. The discharge, pulsed valve, and ICCD are all triggered by a DG535 pulse generator for synchronization.

3.3 Two main emission stages

It is observed that from the outset of discharge, the process of fluorescence can be divided in time into two different stages with starkly different features. The first stage starts with the rising of the high-voltage pulse and

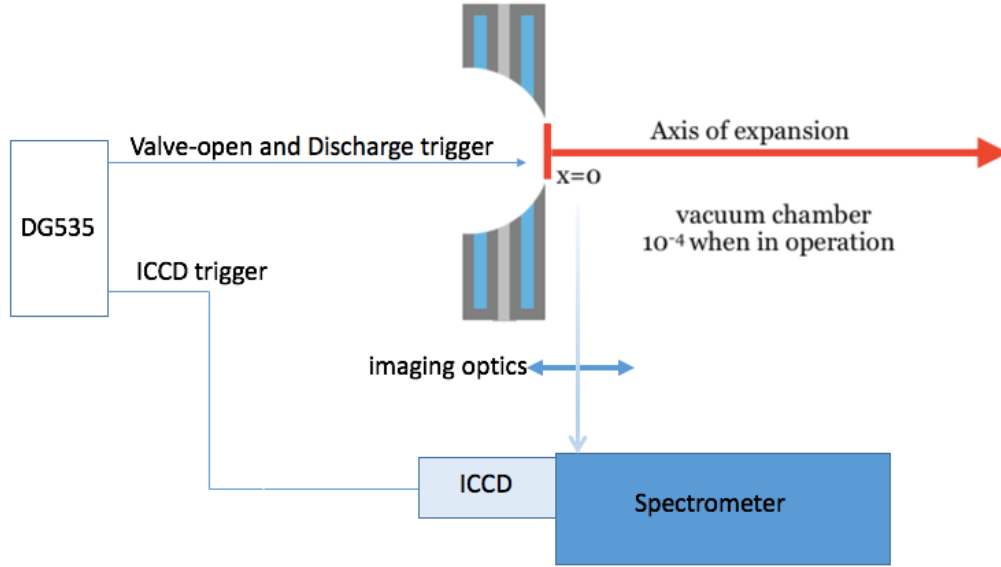


Figure 3.2: Schematic diagram of the experimental arrangement (dimensions not to scale). 2 kV voltage with short duration and fast rise time is applied across the device at 10 Hz. The pressure of the gas is 4 atm. Discharge, pulsed valve and ICCD are synchronized by a DG535 pulse generator. The axis of the expansion is imaged in parallel onto the input slit of the spectrometer.

is characterized by a burst of fluorescence with relatively strong intensities observed on the ICCD array without the use of a spectrometer. The fluorescence spreads across the whole array within tens of nanoseconds, indicating a propagating speed on the order of several kilometers per second. This speed does not correspond to the propagation speed of the atoms of the gas and thus is attributed to the burst of electrons released from the outset of discharge. These electrons impact the existed atoms in the vacuum (the valve has been opened before the arrival of discharge), and excited atoms contribute to the burst of fluorescence. It is safe to say that no emission from excited dimers is present in this strong fluorescence after we checked the emitted spectrum.

This initial burst of atomic fluorescence fades within several hundreds of nanoseconds and a second kind of fluorescence starts roughly 230 ns after the arrival of the voltage, even though the atomic emission at this time is not completely gone. ICCD monitoring shows that this second stage of fluorescence propagates at a speed much slower than the first and is consistent with the propagating speed of gas atoms. The spectrogram shows that

transitions between different electronic states in helium dimer contributed to this stage of fluorescence. Especially, $d^3\Sigma_u^+ \rightarrow b^3\Pi_g(v', v'') = (0, 0)$, $f^3\Sigma_u^+ \rightarrow b^3\Pi_g(v', v'') = (0, 0)$, and $e^3\Pi_g \rightarrow a^3\Sigma_u^+(v', v'') = (0, 0)$ emissions are captured on ICCD array. Figure 3.3 shows the spectrogram of $d^3\Sigma_u^+ \rightarrow b^3\Pi_g(v', v'') = (0, 0)$ emission. These spectrograms not only prove the generation of these electronic states in helium dimers, but also provide the information about their temporal-spatial evolution during the cooling process, which we will analyze in Chapter 4.

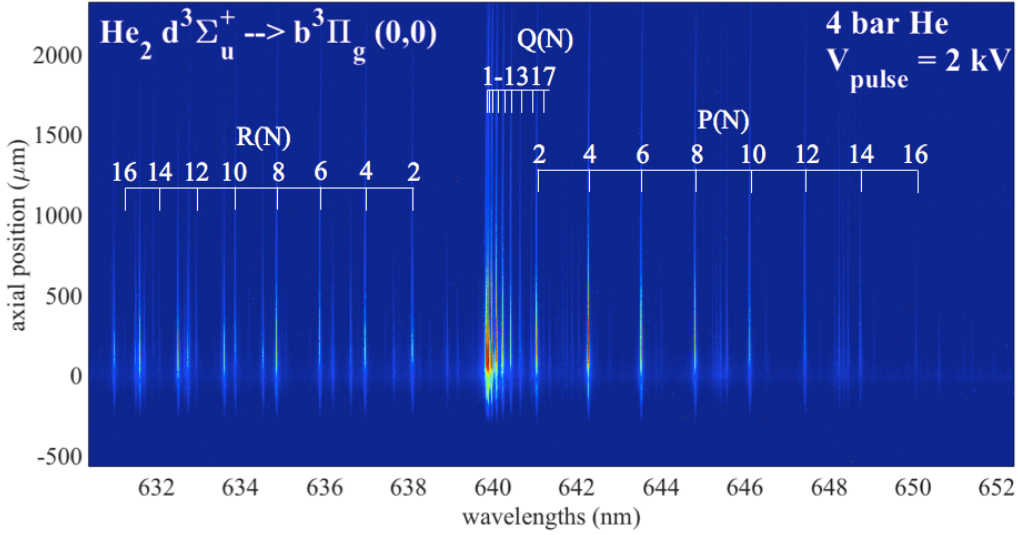


Figure 3.3: False color spectrogram image shows the temporal-spatial evolution of the rotationally resolved $d^3\Sigma_u^+ \rightarrow b^3\Pi_g(v', v'') = (0, 0)$ emission along the axis of supersonic expansion.

3.4 Emission spectrogram of helium dimers

From the spectrogram of $d^3\Sigma_u^+ \rightarrow b^3\Pi_g(v', v'') = (0, 0)$ emission in Figure 3.3, we can see that lines P(2), P(4), P(6), ...P(16) are clearly resolved and identified, as are the Q(1), Q(2), Q(3), ...Q(17) for the Q branch and the R(2), R(4), R(6), ... R(16) for the R branch. This means that for the $d^3\Sigma_u^+ \rightarrow b^3\Pi_g(v', v'') = (0, 0)$ transitions, the physical information about the upper rotational levels up to $N = 15$ can be deduced from the spectrum. The full-width-half-maximum (FWHM) of each line is no more than 0.4 \AA , which

is less than 1 cm^{-1} around a center wavelength of 640 nm. The exact positions of these identified lines are compared with those in Ginter's paper [7] and for most lines, the difference from values in the literature is no more than 1.5 cm^{-1} . In fact, the resolution of the spectrum we got here is high enough that on the ICCD array 75% of the peak intensity for one line falls only within three pixels. This is good for identifying the wavelength of each line but can increase the error when we do a lineshape fitting (the more meaningful data points used, the better the model fitting result). It is therefore more beneficial to purposely decrease the spectrometer resolution by defocusing the ICCD in the situation of model fitting.

Also resolved in the experiment but not shown here are the emission spectra of $f^3\Sigma_u^+ \rightarrow b^3\Pi_g(v', v'') = (0, 0)$ and $e^3\Pi_g \rightarrow a^3\Sigma_u^+(v', v'') = (0, 0)$ transitions.

It is worthwhile to note that these spectrograms captured not only the spectrum at one moment in the dynamic progress, but recorded the spectrum at every single moment and location downstream of the nozzle where the molecules traveled. They are, therefore, temporal-spatial spectrograms that contain the information about the evolution of the populations at different energy levels of He_2 during the expansion.

CHAPTER 4

ANALYSIS

4.1 Rotational temperature analysis of He₂

$d^3\Sigma_u^+ \rightarrow b^3\Pi_g(v', v'') = (0, 0)$ emission

As we have mentioned at the end of Chapter 3, each row of pixels on the spectrogram of Figure 3.3 represents the spectrum of the fluorescence emitted by the molecules when the molecules travel to that location. Figure 4.1 shows two rows of the spectrum, the P branch of the He₂ $d^3\Sigma_u^+ \rightarrow b^3\Pi_g(v', v'') = (0, 0)$ emission at location 5 μm (red) and 250 μm (blue) away from the exit of the device, respectively.

Two things have been brought to our attention. Firstly, the relative intensities of different lines change drastically between the spectra captured at two different locations. For example, when the excited molecules are 5 μm away from the nozzle, the P4 line is stronger than the P2 line. When the same cluster of molecules travel to the location 250 μm away from the nozzle, however, the P2 line becomes stronger than the P4 line, indicating a lower value of rotational temperature than that at 50 μm . More generally, the change in the intensity envelope of the lines from P2 to P16 reflects cooling in the rotational temperature. Secondly, even for the spectra at one single location, for example, the 250 μm one (blue), the intensity envelope of the P branch does not follow a smooth Boltzmann distribution profile because P10 and P12 have higher intensities than those expected from a Boltzmann distribution, while the intensities of P14 and P16 drop abruptly. In other words, the distribution of the population in different rotational levels cannot be described by a single temperature under Boltzmann distribution. In order to model the change in temperature as the molecules travel in a vacuum, we use a modified Boltzmann distribution characterized by two rotational temperatures, in which the intensity $I(N')$ of the transition from upper level N'

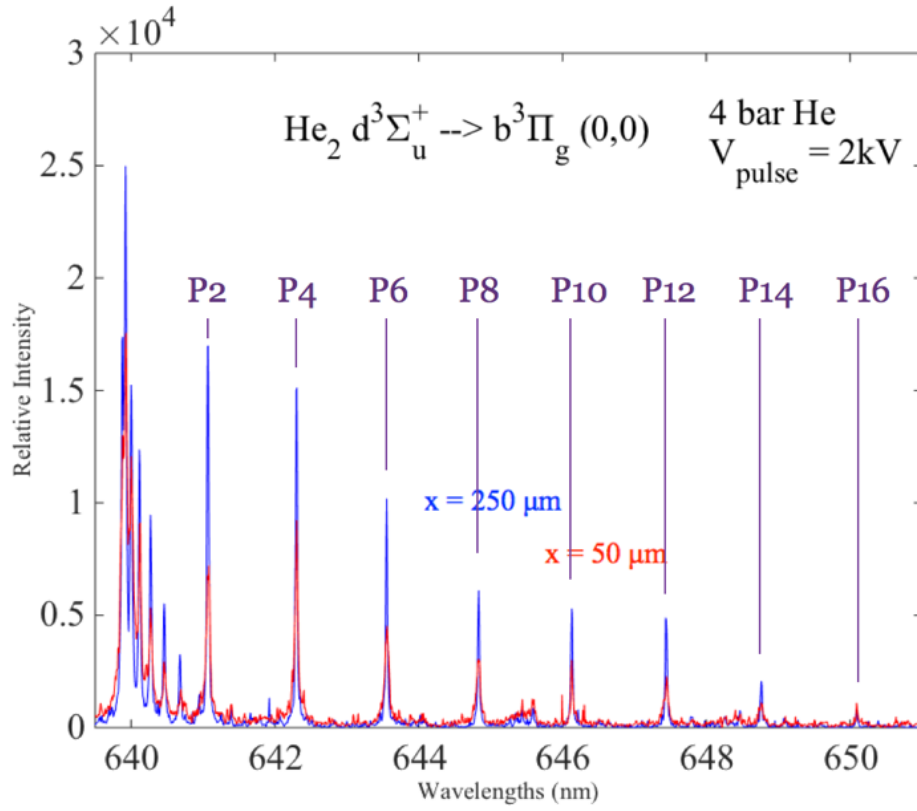


Figure 4.1: P branch of the He_2 $d^3\Sigma_u^+ \rightarrow b^3\Pi_g(v', v'') = (0, 0)$ emission at location $50 \mu\text{m}$ (red) and $250 \mu\text{m}$ (blue) downstream of the nozzle. Notice the change in rotational distribution at two different locations. On the left of the P branch are the lines of the Q branch for which not all lines are labeled in the figure.

is given by,

$$I(N') = S(N')(\kappa_1 e^{-\frac{B'_0}{kT_1} N'(N'+1)} + \kappa_2 e^{-\frac{B'_0}{kT_2} N'(N'+1)}) \quad (4.1)$$

where $S(N')$ is the “line-strength” factor as a function of N' for the P branch, B'_0 is the rotational constant of the upper vibrational level $v' = 0$, κ_1 and κ_2 are two constants weighing the contribution from each temperature T_1 and T_2 .

With the aforementioned model, MATLAB is employed to fit rotational temperatures to each row of the spectrum in Figure 3.3. Figure 4.2 plots the fitting result of one set of data.

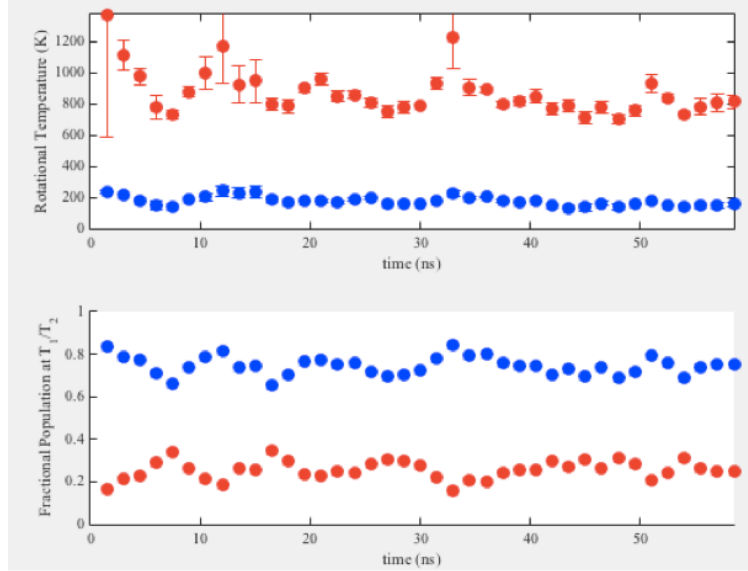


Figure 4.2: Temporal evolution of the fitted rotational temperatures along the axis of expansion.

The top section of Figure 4.2 presents the two fitted temperatures as a function of traveling time (or distance away from the nozzle) and the bottom section presents the fractional population of the molecules that can be characterized by the corresponding temperature, given by $\kappa_1/(\kappa_1 + \kappa_2)$ and $\kappa_2/(\kappa_1 + \kappa_2)$. Although the molecules do not travel at a constant speed after they leave the nozzle, a rough approximation can be made that they travel $2\sim 3 \mu\text{m}$ per nanosecond on average. Error bars are marked on the figure for the fitted temperatures. The cooling effect is affirmed from the result of this fitting; the high temperature, which accounts for less than 40% of the

population, decreases drastically from more than 1000 K to 800 K within 30 ns while the low temperature that accounts for a larger population, decreases from about 250 K to around 100 K. In order to verify the repeatability, more sets of data are taken on different dates and on different parts of the ICCD array. Similar fitting results are consolidated in Figure 4.3. For certain sets of data, cooling of high temperature to ~ 600 K and low temperature to below ~ 100 K is achieved.

4.2 Damped harmonic oscillation in rotational temperature cooling

Figure 4.3 shows four sets of the temporal evolution of the low temperature (top) and high temperature (bottom) along the axis of expansion. Not only do they share the same trend of cooling, but the temperatures follow a damped oscillation profile in all sets of data. Noticing that the four sets of data are taken on different dates and on different parts of the ICCD array, which eliminates the possibility of intrinsic modulation on the ICCD array. Considering the configuration of the device, we attribute this observed sinusoidal trend to the reflection of electrons from a virtual cathode located downstream of the expansion. This is illustrated in Figure 4.4.

Recalling the discussion of “the first emission stage” in Section 3.3, upon the discharge, the electrons are accelerated and repelled by the cathode into vacuum at a very fast speed. However, the electric field in the vacuum points away from the nozzle because of the location of the anode. For the electrons that do not have enough kinetic energy to overcome the potential barrier, they reach the virtual cathode and then travel back to the nozzle. The electrons thus move back and forth between two cathodes and heat up the traveling molecules whenever they encounter them. This heating mechanism adds onto the supersonic cooling effect for the helium dimers, resulting in a damped sinusoid profile as shown in Figure 4.3 or the enlarged Figure 4.5. On an attempt to verify our conjecture, we try to fit the rotational temperatures to a damped harmonic oscillation model, which is discussed as follows. The basic formula that governs a harmonic oscillation is given by,

$$\ddot{x} + 2\gamma\dot{x} + \omega_0 = 0 \quad (4.2)$$

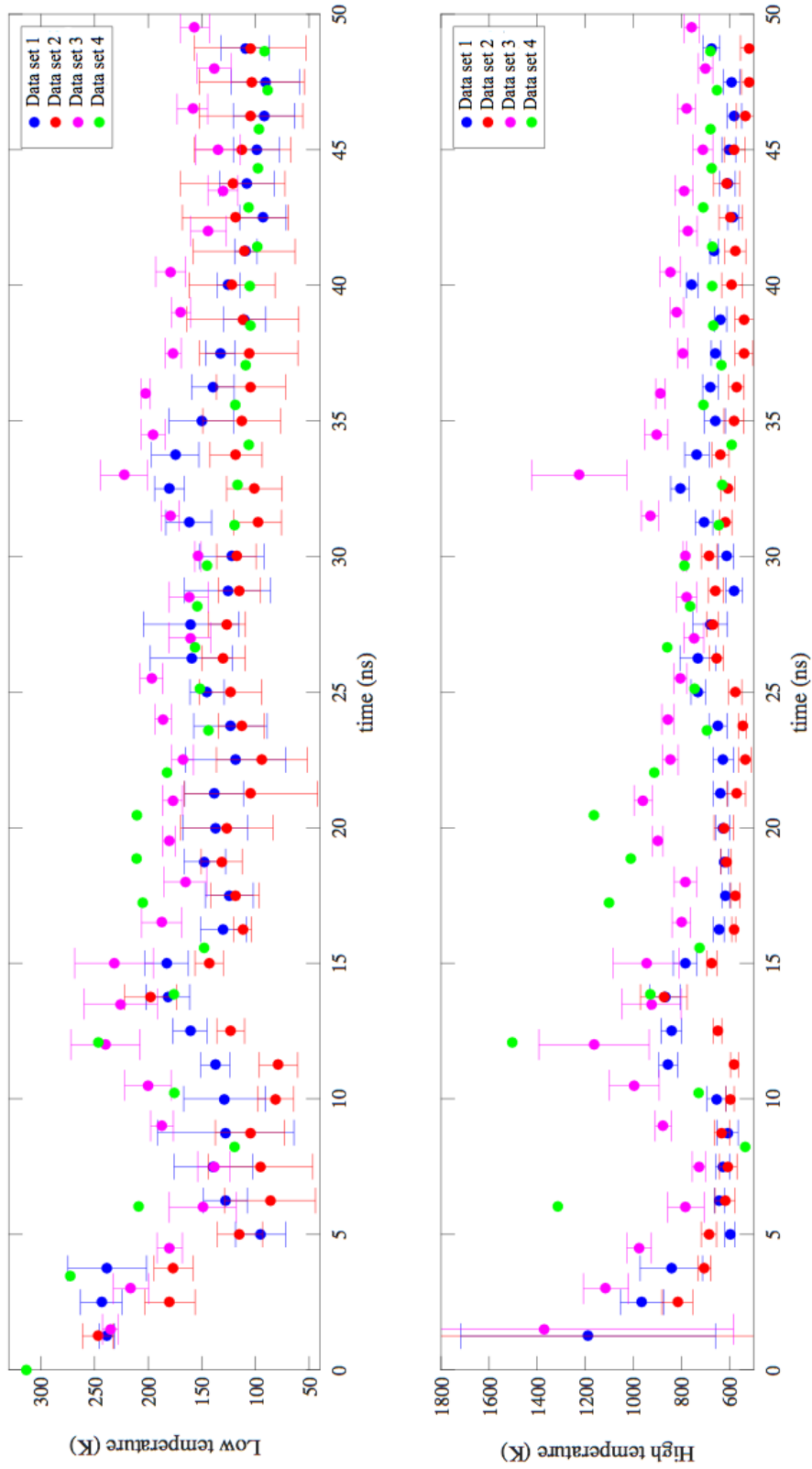


Figure 4.3: Temporal evolution of rotational temperatures along the axis of expansion fitted from spectrograms taken on different dates and on different parts of the ICCD array. Notice that they follow similar trends of cooling and the damped sinusoidal feature.

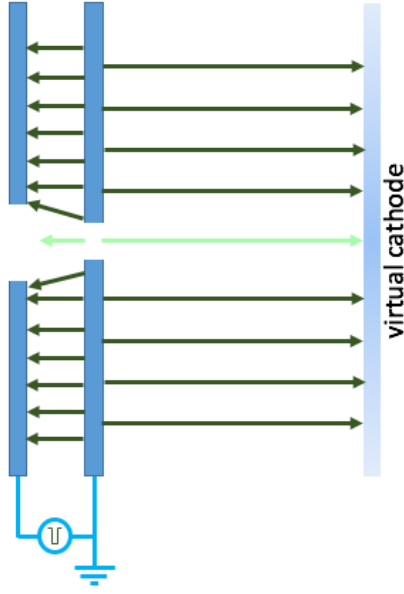


Figure 4.4: Electrode configuration of the microplasma device and the virtual cathode in the vacuum. Green lines represent the directions of the electric field.

where γ is the damping factor, ω_0 is the oscillation frequency, and x is the physical variable that oscillates, for example, the location of a particle or the rotational temperature T that reflects the oscillated motion of the electrons. Assuming ω_0 to be the plasma frequency and substituting T for x , we can solve Equation 4.2 and get,

$$T(t) = T_0 e^{-\gamma t} \cos(\omega_0 t) \quad (4.3)$$

The result of the fitting and the data points used are shown in Figure 4.5. Within 25 ns of the molecules' expansion, the evolution of rotational temperature fits well to a damped sinusoid, yielding a plasma frequency of about 5×10^8 Hz, which corresponds to an electron density of $7 \times 10^7 \text{ cm}^{-3}$. This value might look small at first glance. However, since the “second stage of emission” as described in Section 3.3 happens about hundreds of nanoseconds after the initial burst of the electrons, the electrons that still participate in the oscillation at the second stage may not be as numerous as those within the plasma device initially.

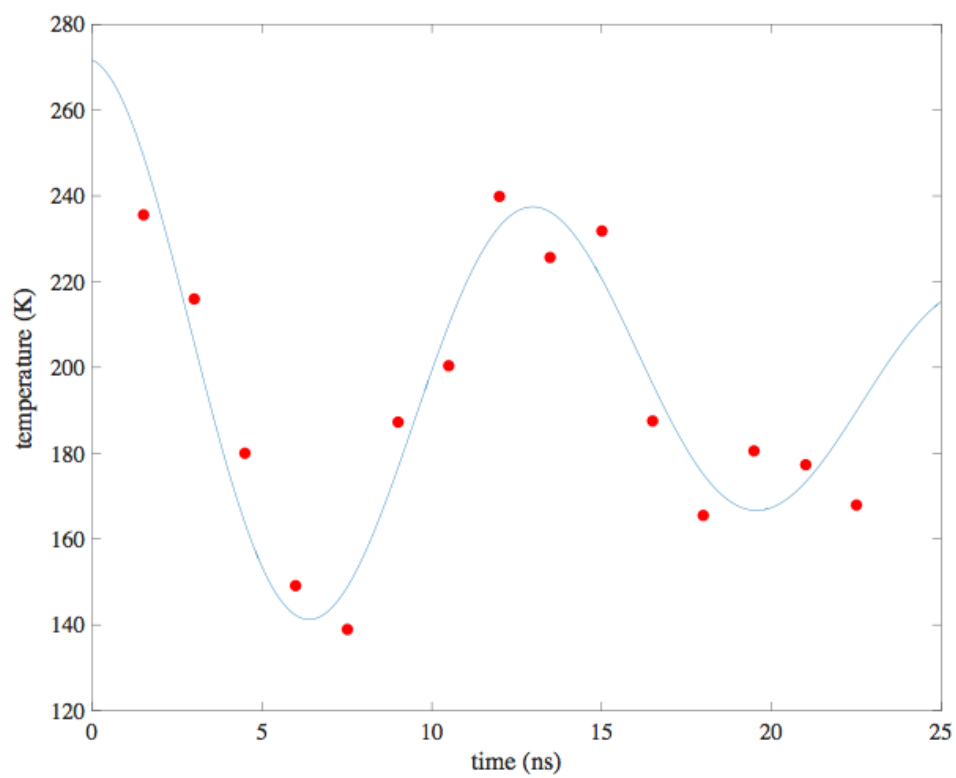


Figure 4.5: Damped sinusoid fitting (solid line) of the rotational temperatures of the molecules within the travel of 25 ns away from the nozzle.

CHAPTER 5

CONCLUSIONS

An experimental technique that combines a microcavity plasma device and supersonic expansion has been demonstrated. Electronic states in helium dimers that have high excitation energies and short lifetimes have been generated and studied. For the $d^3\Sigma_u^+ \rightarrow b^3\Pi_g(v', v'') = (0, 0)$ emission, the rotationally resolved spectrum has been recorded on a temporal-spatial axis of the expansion, enabling the study of plasma dynamics in time and space. It has been found that the rotational temperature of the ground vibrational state of the electronic state $d^3\Sigma_u^+$ is effectively cooled. The temperature that describes the majority of the population has been cooled below 100 K. The temporal evolution of the rotational temperature features a damped sinusoid, which we attribute to the repelling of electrons by a virtual cathode located downstream of the nozzle. With this physical model, numerical fitting yields an electron density of $7 \times 10^7 \text{ cm}^{-3}$, the reasonability of which is discussed.

Beyond work presented in this thesis, the presented experimental technique is expected to facilitate the study of molecular spectroscopy and plasma dynamics, especially for the electronic states that are hard to obtain from the ground using optical methods. Also of value is the technique's ability of temperature cooling and that the collisions happening through the process are desired in various physical processes such as rotational relaxation or population transfer among different electronic states. In this light, future work may be to extend this technique to the study of physical processes in other molecules, such as Ne_2 , Ar_2 , N_2 or CO_2 . For the He_2 , since we are able to compress the population into certain rotational levels through the cooling process while monitoring, future work may also involve using lasers to manipulate the population of a specific rotational level.

REFERENCES

- [1] R. Campargue, Ed., *Atomic and Molecular Beams: The State of the Art 2000*. Springer Science & Business Media, 2012.
- [2] A. Kantrowitz and J. Grey, “A high intensity source for the molecular beam. Part I. Theoretical,” *Review of Scientific Instruments*, vol. 22, no. 5, p. 328, 1951.
- [3] K. H. Becker, K. H. Schoenbach, and J. G. Eden, “Microplasmas and applications,” *Journal of Physics D: Applied Physics*, vol. 39, no. 3, pp. R55–R70, 2006.
- [4] F. Paschen, “Bohrs heliumlinien,” *Annalen der Physik*, vol. 355, no. 16, pp. 901–940, 1916.
- [5] A. D. White, “New hollow cathode glow discharge,” *Journal of Applied Physics*, vol. 30, no. 5, pp. 711–719, 1959.
- [6] M. D. Morse, “2. Supersonic beam sources,” *Atomic, Molecular, and Optical Physics: Atoms and Molecules. Series: Experimental Methods in the Physical Sciences*, vol. 29, pp. 21–47, 1996.
- [7] M. L. Ginter, “Potential-energy curves for the He_2 molecule,” *The Journal of Chemical Physics*, vol. 52, no. 9, p. 4469, 1970.
- [8] P. W. Atkins and J. De Paula, *Atkins’ Physical Chemistry*. Oxford University Press, 2010.
- [9] G. Herzberg, *Molecular Spectra and Molecular Structure. Vol. 1: Spectra of Diatomic Molecules*. D. Van Nostrand Company, Inc., 1950.
- [10] J. H. Cho, M. H. Kim, S. J. Park, and J. G. Eden, “Arrays of microplasma jets generated by double parabolic microcavities in an hour-glass configuration,” *IEEE Transactions on Plasma Science*, vol. 39, no. 11, pp. 2376–2377, 2011.
- [11] J. H. Cho, S.-J. Park, and J. G. Eden, “Propagation and decay of low temperature plasma packets in arrays of dielectric microchannels,” *Applied Physics Letters*, vol. 101, no. 25, p. 253508, 2012.